Purdue University

Purdue e-Pubs

3-1-2023

Mapping the amplitude and frequency of pressure drop oscillations via a transient numerical model to assess their severity during microchannel flow boiling

Md Emadur Rahman
rahman85@purdue.edu

Justin Weibel
jaweibel@purdue.edu

Follow this and additional works at: https://docs.lib.purdue.edu/coolingpubs

Mapping the Amplitude and Frequency of Pressure Drop Oscillations via a Transient Numerical Model to Assess their Severity during Microchannel Flow Boiling

Md Emadur Rahman**,** Justin A. Weibel*

Cooling Technologies Research Center, School of Mechanical Engineering,
Purdue University, West Lafayette, IN 47907 USA

*Corresponding author.

Email address: rahman85@purdue.edu (Md E. Rahman), jaweibel@purdue.edu
(Justin A. Weibel)

Abstract: Flow boiling in microchannel heat sinks offers effective cooling for high-power electronics devices and compact heat exchangers in many other industrial applications. However, flow boiling instabilities, in particular pressure drop oscillations, can occur in these heat sinks and may reduce their performance by causing premature initiation of critical heat flux (CHF) or deterioration of the heat transfer coefficient. Predicting the occurrence and severity of pressure drop oscillations is hence important to ensure reliable operation. We perform stability analysis using bifurcation theory to determine the effect of various operating and geometric parameters on these oscillations in microchannel heat sinks. The analysis identifies the unstable (where pressure drop oscillations occur) and stable regions of operation based on the mass flux, heat input, and amount of inlet restriction. As the stability map does not yield information regarding the severity of oscillations in the unstable region, the effects of these parameters on the amplitude and period of pressure drop oscillations are also assessed via a transient numerical model. Surveying these parameters over the unstable region allows assessment of potential performance reductions of the heat sink due to pressure drop oscillations.

Keywords: Microchannel heat sink; flow boiling instability; pressure drop oscillations; stability analysis; two-phase flow

Nomenclature

A_c	Channel cross-section area (m^2)
A_p	Pipe cross-section area (m^2)
C	Chisholm parameter
D_h	Hydraulic diameter (m)
D_p	Pipe diameter (m)
F_w	Frictional pressure gradient
f_ϕ	Friction factor $\left(2\frac{\tau_w \rho_\phi}{G_{in}^2}\right), \phi = f, g$)
G	Mass flux (kg/m^{2}s)
G_{buf}	Mass flux to buffer tank (kg/m^{2}s)
G_{in}	Mass flux to channel (kg/m^{2}s)
G_{in}^*	Equilibrium mass flux to channel (kg/m^{2}s)
h	Enthalpy (kJ/kg)
h_{in}	Inlet enthalpy of liquid (kJ/kg)
h_f	Saturation enthalpy of liquid (kJ/kg)
h_g	Enthalpy of vapor (kJ/kg)
h_{fg}	Enthalpy of vaporization (kJ/kg)
H_c	Height of channel (m)
I	Identity matrix
J	Jacobian matrix
K	Inlet throttle resistance coefficient (-)
L_c	Length of channel (m)
p	Pressure (Pa)
P_{atm}	Atmospheric pressure (Pa)
P_{buf}	Buffer tank pressure (Pa)
P_{buf}^*	Equilibrium buffer tank pressure (Pa)
P_i	Initial pressure of compressible volume (Pa)

Re	Reynolds number $\left(\frac{G_{in}D_h}{\mu}\right)$
Re_f	Superficial liquid Reynolds number $\left(\frac{(1-x)GD_h}{\mu_f}\right)$
Re_g	Superficial vapor Reynolds number $\left(\frac{xGD_h}{\mu_g}\right)$
q'	Heat input per channel length (W/m)
T_{in}	Inlet temperature (°C)
T_{sat}	Saturation temperature (°C)
t	Time (s)
u	Velocity (m/s)
V	Total buffer tank volume (m³)
V_{buf}	Compressible volume (m³)
V_f	Liquid volume inside buffer tank (m³)
V_i	Initial compressible volume (m³)
v	Specific volume (m³/kg)
W_c	Width of channel (m)
x	Vapor quality $\left(\frac{h-h_f}{h_g-h_f}\right)$
z	Coordinate along channel length (m)
ΔP	Pressure drop (Pa) $\left(P_{buf} - P_{atm}\right)$
ΔP_A	Acceleration pressure drop (Pa)
ΔP_F	Frictional pressure drop (Pa)
ΔP_G	Gravitational pressure drop (Pa)
Δh_{in}	Enthalpy difference (kJ/kg) $\left(h_f - h_{in}\right)$
$\delta(z - L_c)$	Kronecker delta function
δG_{in}^*	Perturbation of mass flux (kg/m²s)
δP_{buf}^*	Perturbation of buffer tank pressure (Pa)
$\left(\frac{\partial p}{\partial z}\right)_f$	Liquid frictional pressure gradient $\left(2f_f \frac{v_f(1-x)^2G^2}{D_h}\right)$
$\left(\frac{\partial p}{\partial z}\right)_g$	Vapor frictional pressure gradient $\left(2f_g \frac{v_g x^2 G^2}{D_h}\right)$

Subscripts

A	Acceleration
F	Friction
f	Liquid
G	Gravitation
g	Vapor

Greek symbol

α	Void fraction
β	Aspect ratio of channel $\left(\frac{W_c}{H_c}\right)$
λ	Eigenvalues
λ_R	Real part of eigenvalues
μ_f	Liquid dynamic viscosity (Pa·s)
μ_g	Vapor dynamic viscosity (Pa·s)
ρ_f	Liquid density (kg/m³)
ρ_g	Vapor density (kg/m³)
τ_w	Shear stress (Pa)
ω	Imaginary part of eigenvalues

1   Introduction

Two-phase flow heat transfer is currently relied upon in various industrial applications such as chemical evaporators, steam generation, thermosiphons, nuclear power plants, and air conditioning systems [1,2]. The next-generation of high-power electronic devices used in communications, computing, and power conversion systems will generate localized heat fluxes on the order of ~1 kW/cm² [3,4]. Heat must be effectively removed to keep these devices at the desired operating temperatures required for performance, efficiency, and reliability. Traditional air-cooling technologies are straightforward in their implementation, but may be limited to dissipation of lower heat fluxes in compact spaces [5]. Microchannel flow boiling heat sinks offer a compact alternative owing to high heat transfer coefficients and requires lower pumping power compared to single-phase liquid cold plates. Therefore, this approach is being actively explored for the

cooling of advanced electronic semiconductor devices, electric machines and drives in vehicles and aircraft, and lithium-ion batteries, to name a few [6,7]. However, one practical challenge associated with the implementation of microchannel flow boiling heat sinks is their susceptibility to flow instabilities that may reduce operational performance compared to design predictions if not considered.

The various flow instabilities observed in microchannel heat sinks can be broadly classified into two categories, static and dynamic instabilities, which have been reviewed extensively in the literature [1,2]. A well-known and frequently observed static instability is the flow excursion or Ledinegg instability [8]. Due to this instability, which is governed based interaction between the flow boiling channel pressure drop versus mass flux (demand curve) and pump curve characteristics, a microchannel can experience a sudden change in mass flux from its initial operating condition. A sudden change to a lower mass flux, and commensurate higher exit vapor quality, may cause premature critical heat flux. In networks of multiple parallel channels, this instability can lead to steady maldistribution of the flow [9–12]. Commonly identified dynamic instabilities include density wave oscillations, parallel channel instabilities, and pressure drop oscillations. Dynamic instabilities occur inside the channel because of feedback interactions between various effects such as inertia and compressibility of the flow. In microchannel heat sinks, pressure drop oscillations are of particular concern as sustained large amplitude and low frequency oscillations of mass flux and pressure have been observed to occur [2,13,14]. Hence, pressure drop oscillations can initiate premature critical heat flux (CHF), cause mechanical vibrations, and deteriorate the heat transfer coefficient [1,15]. The focus of the current study is investigation of pressure drop oscillations in microchannel heat sinks, with particular emphasis on stability analysis techniques and offering prediction of the amplitude and period of such oscillations.

1.1   Pressure drop oscillation mechanism

Pressure drop oscillations generally occur in the microchannel heat sinks when the demand curve (pressure drop versus mass flux) has a negative slope region and there exists an upstream compressible volume [1,2,16]. Such compressible volume is difficult to unconditionally avoid as it can arise from trapped noncondensables, plenums, or slight mechanical compliance, rendering microchannel heat sinks prone to pressure drop oscillations [14]. A representative flow boiling demand curve for fixed heat input and subcooled inlet temperature has a non-monotonic N-shape, as shown in Figure 1(a) (see the blue dotted line). This curve is labelled based on three regions

where the outlet is a subcooled liquid phase, a vapor-liquid two-phase mixture, or superheated vapor phase. At a high mass flux, the heat input is insufficient to bring the liquid up to the saturation temperature at the outlet; hence, the channel contains only liquid and the pressure drop decreases with decreasing mass flux due to lesser friction. As the mass flux decreases, the liquid eventually reaches the saturation temperature and will begin to generate vapor at the microchannel outlet. The demand curve reaches a local minimum pressure drop at this mass flux. The pressure drop increases with further decreases in mass flux due to increased friction and acceleration of the flow by vapor generation, leading to a negative slope region. As the mass flux further decreases, the pressure drop begins to decrease (positive slope in the demand curve) as a majority of the channel length is single-phase vapor upstream of the outlet. The demand curve has a local maximum during this transition between regions.Figure 1(a) shows that the demand curve (blue dotted line) intersecting with a source of constant mass flux G_{buf} (vertical dashed line) within the negative slope region. This constant mass flux supply is representative of a positive displacement pump. The intersection point (red circle) is stable with respect to the Ledinegg instability due to the relative slope of the demand curve being algebraically smaller than the slope of the supply curve [1,2]. Although the point is stable for the Ledinegg instability, pressure drop oscillations may still occur at this point in the presence of upstream compressible volume (such as for the system with an upstream buffer tank as shown in Figure 1(b)). Pressure drop oscillations (PDO) follow a time-periodic limit cycle around the desired operating point, following the representative dynamic path (solid green line) of mass flux (G_{in}) versus pressure drop ($\Delta P = P_{buf} - P_{atm}$) traced over the channel load curve in Figure 1(a). The PDO mechanism is triggered for an unstable system by a small disturbance in mass flux when intending to operate at the pump-demand intersection point (red circle), and can be explained by following along the dynamic path from A to D. From D to A, the instantaneous mass flux into microchannel heat sink (G_{in}) is more than the mass flux into the buffer tank (G_{buf}), so the height of the liquid level and pressure in the buffer tank decrease. At point A, the low available pressure difference cannot supply such a high mass flux into the heat sink per the channel demand curve characteristics. Hence, a jump occurs from a low outlet vapor quality at point A to a high vapor quality at point B. From B to C, the mass flux into the buffer tank is greater than mass flux into the channel, so the buffer tank pressure and thereby total pressure drop (ΔP) increases. At point C, the overly high pressure causes an excursion from a superheated vapor outlet at point C to a subcooled liquid outlet at point D, and the process repeats continuously.

6
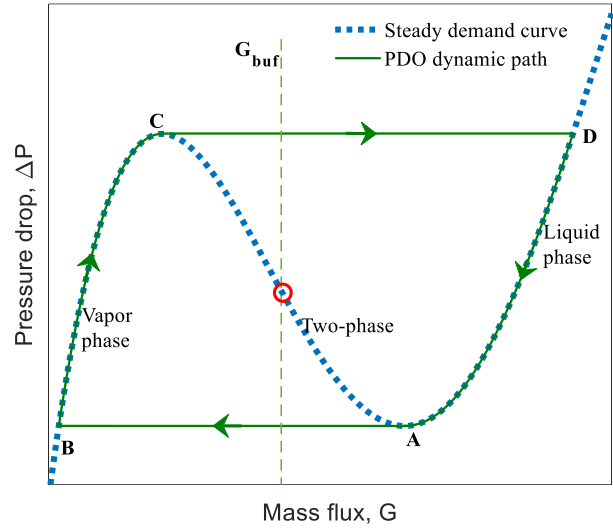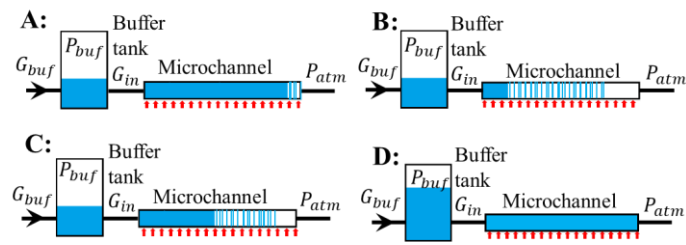
Figure 1 (a) Typical *N*-shape steady demand curve (blue dotted line) for flow in a heated channel. The curve is annotated with a dashed vertical line for the constant mass flux (into buffer tank, G_{buf}) point of desired operation and green line overlay tracing the pressure drop oscillation (PDO) dynamic path during where mass flux into microchannel (G_{in}) varies. (b) Schematic diagrams of the system, a heated microchannel with an upstream compressible volume, with the instantaneous fluid states in the buffer tank and microchannel shown the locations A, B, C, and D along the PDO limit cycle (liquid in solid blue, two-phase mixture hashed, and vapor in solid white).

Per the pressure drop oscillation mechanism, the result is a fluctuation between high and low mass fluxes (above and below the desired operating point) inside the microchannel. The significance of oscillating mass flux is the potential implications on the heat transfer performance. First, at the relatively high mass fluxes from D to A, a majority of the fluid along the channel length remains subcooled liquid and dissipates heat by single-phase convection at a reduced heat transfer coefficient compared to the desired operating point. Next, at the comparatively low mass

7

flux from B to C, the channel length contains a two-phase mixture with a superheated vapor outlet. Heat transfer may deteriorate significantly in the superheated regions, and at worst, this could initiate critical heat flux (CHF). Apart from the possible triggering of CHF, such oscillations of mass flux and pressure in the microchannel raise reliability concerns associated with nonuniform oscillations in temperature or vibrations.

1.2   Literature survey

Several experimental studies have been carried out to understand the effects of pressure drop oscillations (viz., mass flux, pressure, and thermal oscillations) on the heat transfer coefficient and CHF in microchannel heat sinks [13,17–20]. Several of these studies [17,18,20] have found that the pressure drop and temperature oscillations significantly deteriorate the heat transfer performance of the heat sinks due to these oscillations. Whereas other recent work, such as Ref. [19] using HFE-7100 as coolant fluid, reports relatively minor effects on the heat transfer coefficient in the presence of mass flow rate and pressure oscillations. Modeling approaches are needed for understanding these effects of pressure drop oscillations on microchannel heat sinks, which may strongly depend on application-specific factors such as the fluid properties, heat sink geometry, and operating conditions. Stability analysis is used to map the occurrence of oscillations over a range of parametric operational space (i.e., heat input, mass flux, inlet subcooling, etc.) and can potentially detect their effect on heat transfer coefficient or CHF.

Researchers have therefore developed various modeling approaches to predict these instability phenomena [16,21–24]. Padki et al. [21] created a lumped model (i.e., integrated over channel length to yield governing ordinary differential equations only as a function of time) to predict the occurrence of pressure drop oscillations and the Ledinegg instability using a bifurcation analysis. They reported that a Hopf bifurcation confirms the occurrence of pressure drop oscillations, and a saddle-node bifurcation confirms the Ledinegg instability. Other studies [22,25,26] investigate pressure drop oscillations using nonlinear stability analysis. Rahman et al. [25] used a lumped-parameter model to identify the Ledinegg instability, pressure drop oscillations, and a unique flow excursion with compressible volume (FECV), while varying external pump characteristics. The seminal work by Zhang et al. [16] developed a model to identify the pressure drop oscillations, and compared against experimental observations. This study further offered a method to determine the amount of compressibility present in the system when there is no external buffer tank and devised a scheme for model-based active control to address pressure drop oscillations in

8

microchannel heat sinks. Eborn [27] proposed a control method to suppress pressure drop oscillations based on the liquid-to-vapor density ratio in the microchannel heat sink. The method derived a condition that, if the density ratio is lower than certain critical threshold, then the negative slope in the demand curve will vanish and there will be no occurrence of pressure drop oscillations. Zhang et al. [23] extended this approach by using the system pressure to suppress pressure oscillations, in addition to the conventional passive control technique of using inlet restrictors for flow stabilization. Kuang et al. [24] simplified the evaluation of the pressure drop using a functional approximation to identify the stable and unstable operating regions based on a subcooling number and phase change number. The effect of gravity on the stability of microchannel heat sinks was also discussed; the system has a larger stable region with higher gravity.

Stability analyses are useful to identify the regions of operation (e.g., heat input, inlet temperature, mass flux) over which instabilities occur. But these do not necessarily describe the severity of the dynamics, such as the amplitude and period of oscillations, that primarily affect the heat transfer coefficient [28]. In the regions where pressure drop oscillations are predicted to occur in microchannel heat sinks, the literature lacks quantitative discussion of amplitude and period of the oscillations. Such investigation into the oscillation severity is necessary to draw correlations between the occurrence of pressure drop oscillations and deterioration in the heat transfer coefficient, as has been observed under certain experimental conditions. In addition, stability analysis using nonlinear or bifurcation techniques have not been applied in the context of microchannel heat sinks. The present work uses bifurcation theory to assess flow boiling stability in a microchannel heat sink with upstream compressible volume. In the range of operation where pressure drop oscillations are predicted to occur, the effect of heat input and inlet throttling on the amplitude and period of oscillations is discussed. Mapping the effects of these parameters on the period and amplitude provides a pathway to determine operational regimes where such instabilities may have lesser or larger effect on the heat transfer performance of the microchannel heat sink.

2 Modeling and analysis approach

Figure 2 shows a schematic diagram of the system. The system has a constant liquid mass flux G_{buf} at the inlet to a partially filled and sealed buffer tank that contains a trapped volume of compressible gas (with properties of air and assuming no species transport between the two phases). There is an inlet throttle (flow resistance coefficient K) between the buffer volume and the channel section representative of a heat sink where a constant and uniform heat input per unit length q' is applied to the flow. Physical parameters are selected for this model system such that they are representative of characteristic dimensions and operating conditions for two-phase microchannel heat sinks in potential electronics thermal management applications. The size of the buffer tank is $V = 40$ ml. The heat sink dimensions and other system operating parameters are given in Table 1. The channel heat input, mass flux to the buffer, and throttle flow resistance coefficient are all kept constant for a given case, but ranges are specified as these parameters are varied later in the study. The coolant used is HFE-7100, a dielectric, low global warming potential, low toxicity, nonflammable, and thermally stable fluid [29]. The thermophysical and environmental properties of HFE-7100 are given in Table 2. In the present work, the model uses constant fluid properties evaluated at saturation conditions at the given outlet atmospheric pressure.
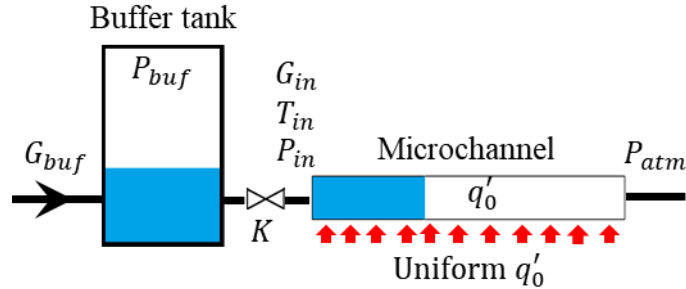

Figure 2 Schematic diagram of the model microchannel heat sink system used to analyze pressure drop oscillations.

Table 1 Dimensions of the microchannel, system parameters, and ranges of operation investigated.

Parameter	Value
Channel length, L_c (mm)	20
Channel width, W_c (µm)	500
Channel height, H_c (µm)	500
Hydraulic diameter, D_h (µm)	500
Pipe diameter, D_p (mm)	2
Size of buffer tank, V (ml)	40
Initial compressible volume (CV), V_i (ml)	35
Initial pressure of CV, P_i (kPa)	101
Heat input per length, q' (W/m)	0-325
Mass flux, G_{buf} (kg/m^{2}s)	0-1100
Throttle flow resistance, K (-)	0-1100
Inlet temperature, T_{in} (°C)	40

Table 2 Thermophysical and environmental properties of HFE-7100 at 1 atm [29].

Property	Value
Saturation temperature, T_{sat} (°C)	60.0
Liquid density, ρ_f (kg/m^3)	1407
Vapor density, ρ_g (kg/m^3)	9.6235
Liquid dynamic viscosity, μ_f (Pa·s)	3.6691×10^{-4}
Vapor dynamic viscosity, μ_g (Pa·s)	1.2157×10^{-5}
Liquid saturation enthalpy, h_f (kJ/kg)	92.776
Enthalpy of vaporization, h_{fg} (kJ/kg)	111.552
Ozone depletion potential (ODP)	0.0
Global warming potential (GWP)	320.0
Atmospheric lifetime ALT (years)	4.1

2.1 Dynamic system model

Transient governing equations are used to analyze the system response and pressure drop oscillations. The model consists of two components, the buffer tank and microchannel heat sink, as shown in Figure 2, and is developed based on the following assumptions [1,21,24,26]:

1. The temperature of the compressible ideal gas in the buffer tank is constant
2. The mass flux into the buffer tank is constant (equivalent to supply from a fixed displacement pump).
3. The instantaneous mass flux through microchannel is uniform
4. The pressure drop between the buffer tank and heat sink inlet is due to the inlet throttle resistance (all other pressure drops in the flow lines are negligible).

The continuity equation of the buffer tank is derived as follows. The difference between the size of the buffer tank, V, and the liquid volume inside the buffer tank, V_f, is the volume of compressible gas, $V_{buf} = V - V_f$ at the pressure defined as P_{buf}. The initial values of volume and pressure of the compressible gas are defined as V_i and P_i, respectively. Then, according to the first assumption of a constant temperature buffer,

$$V_{buf}P_{buf} = V_iP_i \tag{1}$$

differentiating Equation (1) with respect to time and substituting $V_{buf} = V_iP_i/P_{buf}$, yields

$$\frac{dP_{buf}}{dt} = -\frac{P_{buf}^2}{V_iP_i}\frac{dV_{buf}}{dt} \tag{2}$$

Because $V_{buf} = V - V_f$,

$$\frac{dV_{buf}}{dt} = \frac{d(V - V_f)}{dt} = -\frac{dV_f}{dt} \tag{3}$$

Substituting Equation (3) into Equation (2),

$$\frac{dP_{buf}}{dt} = \frac{P_{buf}^2}{V_iP_i}\frac{dV_f}{dt} \tag{4}$$

Given the mass flux into the buffer tank, G_{buf}, and mass flux into the heat sink, G_{in}, the accumulated volume of liquid inside the buffer tank is,

$$\frac{dV_f}{dt} = \frac{(G_{buf}A_c - G_{in}A_c)}{\rho_f} \tag{5}$$

Substituting Equation (5) into Equation (4), the final form of the buffer tank continuity equation becomes,

$$\frac{dP_{buf}}{dt} = P_{buf}^{\;2} \frac{(G_{buf}A_c - G_{in}A_c)}{P_i V_i \rho_f} \tag{6}$$

where A_c is the cross-sectional area of the microchannel.

The one-dimensional partial differential momentum equation of the microchannel heat sink is,

$$\frac{\partial G}{\partial t} + \frac{\partial (Gu)}{\partial z} = -\frac{\partial p}{\partial z} - F_F - F_G - \frac{KA_c^2 G^2}{\rho_f A_p^2}\delta(z - L_c) \tag{7}$$

where the second term on the left-hand side is acceleration pressure gradient, F_F is frictional pressure gradient, and F_G is gravitational pressure gradient. The last term on the right-hand side is pressure drop due to inlet throttle resistance between buffer tank and microchannel heat sink inlet. A lumped dynamic momentum equation for the heat sink is obtained by integrating the momentum equation along the length from buffer tank to heat sink exit,

$$\frac{dG_{in}}{dt} = \frac{1}{L_c}\left(P_{buf} - P_{atm} - \frac{KA_c^2 G_{in}^2}{\rho_f A_p^2} - \Delta P_F - \Delta P_A - \Delta P_G\right) \tag{8}$$

where L_c is the length of the microchannel, P_{atm} the atmospheric pressure, and ΔP_F, ΔP_A, and ΔP_G are the frictional, acceleration, and gravitational pressure drop, respectively.

The right-hand sides of Equations (6) and (8) must be equal to zero at the equilibrium (or steady state) points of the system. The equilibrium points of the system are:

$$P_{buf}^* = P_{atm} + \frac{KA_c^2 G_{in}^{*2}}{\rho_f A_p^2} + \Delta P_F - \Delta P_A - \Delta P_G \tag{9}$$

$$G_{in}^* = G_{buf} \tag{10}$$

where P_{buf}^* is the equilibrium pressure of buffer tank and G_{in}^* is the equilibrium mass flux into the heat sink (in this study, it equals mass flux into buffer tank). These two equilibrium points are used to find the eigenvalues of the Jacobian matrix to identify whether they are stable or unstable (this stability analysis will be discussed ahead in Section 2.3).

2.2 Channel pressure drop

The time period of pressure drop oscillations is typically large compared to the residence time of fluid inside the channel when there is a relatively large compressible volume. For instance, experimentally reported periods of pressure drop oscillations can be 10 s or longer [2,15]. In comparison, for the channel dimensions and fluid properties considered in this work, at a mass flux G_{buf} = 600 kg/(m²s) fluid takes <0.05 s to travel through the entire microchannel length. Hence, any dynamic changes in system operation that occur due to pressure drop oscillations do not instantaneously affect a given particle of fluid, which instead are governed by the quasi-steady-state condition of the channel [16,21,24,26]. Therefore, steady-state approaches are typically implemented to analyze the instantaneous channel pressure drop.

The channel pressure drop (ΔP_c) during two-phase flow of the heated vapor-liquid mixture consists of a frictional pressure drop (ΔP_F), acceleration pressure drop (ΔP_A), and gravitational pressure drop (ΔP_G). In the present analysis, the gravitational pressure drop is neglected (such as in a horizontal microchannel); criteria to assess the importance of gravitational effects in two-phase flows are available [30,31], and this term can be trivially added to pressure drop calculations as needed. A one-dimensional separated flow model is developed to calculate the pressure drop in the microchannel heat sink for this work. This assumes that the vapor and liquid phases have distinct properties and are in local thermal equilibrium (have the same temperature), but the slip ratio may not be equal to 1 (i.e., the liquid and vapor can have different velocities). The flow properties change only in flow direction. Heating from viscous dissipation is neglected for simplicity.

Based on these assumptions, the governing continuity, momentum conservation, and energy conservation equations are respectively written as:

$$\frac{\partial G}{\partial z} = 0 \tag{11}$$

$$\frac{\partial}{\partial z}\left[\left(\frac{v_f(1-x)^2}{1-\alpha} + \frac{v_g x^2}{\alpha}\right)G^2\right] = -\frac{\partial p}{\partial z} - F_F \tag{12}$$

$$\frac{\partial}{\partial z}(hG) = \frac{q'}{A_c} \tag{13}$$

These governing partial differential equations of G, p, and h are solved to obtain the demand curve of the microchannel. The boundary conditions are applied for the one-dimensional flow from the inlet to outlet. At the inlet ($z = 0$), the mass flux is G_{in} and the enthalpy is calculated from the inlet temperature and pressure as $h_{in} = h(T_{in}, p(z = 0))$. At the outlet ($z = L_c$), the pressure is P_{atm}. The thermodynamic equilibrium vapor quality (limited between 0 and 1) is defined as:

$$x = \frac{h - h_f}{h_g - h_f} = \frac{q'z - G_{in}A_c\Delta h_{in}}{G_{in}A_c h_{fg}} \tag{14}$$

The void fraction α is determined using Zivi's correlation [32]:

$$\alpha = \frac{1}{1 + \left(\frac{v_f}{v_g}\right)^{2/3}\frac{1-x}{x}} \tag{15}$$

In the momentum equation (12), the left-hand side defines the acceleration pressure gradient; on the right-hand side, the first term is pressure loss gradient through the channel and the last term is the frictional pressure gradient. The frictional gradient is calculated using the Lockhart-Martinelli method [33]. For the pressure gradient calculation, the formulation by Muzychka and Awad [34] is used:

$$F_w = \left(\frac{\partial p}{\partial z}\right)_f + C\sqrt{\left(\frac{\partial p}{\partial z}\right)_f \left(\frac{\partial p}{\partial z}\right)_g} + \left(\frac{\partial p}{\partial z}\right)_g \tag{16}$$

with the correlation developed by Mishima and Hibiki [35] used for the Chisholm parameter $C = 21[1 - \exp(-319D_h)]$. The single-phase pressure gradients are determined assuming that each phase is present inside the microchannel and occupies the entire cross-section of the channel. Therefore, the liquid and vapor single-phase pressure gradients are respectively:

$$\left(\frac{\partial p}{\partial z}\right)_f = 2f_f \frac{v_f(1-x)^2 G^2}{D_h} \tag{17}$$

$$\left(\frac{\partial p}{\partial z}\right)_g = 2f_g \frac{v_g x^2 G^2}{D_h} \tag{18}$$

where the friction factor f for laminar flow in the rectangular channel is [9]

$$f = \frac{24}{Re}(1 - 1.3553\beta + 1.9467\beta^2 - 1.7012\beta^3 + 0.9564\beta^4 - 0.2537\beta^5) \tag{19}$$

and β is the aspect ratio of the channel within $0 \leq \beta \leq 1$. The Reynolds number of each phase is separately calculated as follows:

$$Re_f = \frac{(1-x)GD_h}{\mu_f} \tag{20}$$

$$Re_g = \frac{xGD_h}{\mu_g} \tag{21}$$

To solve Equations (11)-(13)(14) for G, p, and h, first, the continuity equation yields a trivial solution for the mass flux through the channel of $G(z) = G_{in}$. The remaining two quantities, p and h, are solved using trapezoidal integration with constant fluid properties. The channel of length L_c is discretized into 10^3 nodes.

2.3 Stability analysis

A system is called stable at an operating point if after experiencing a disturbance it returns to this initial operating point; otherwise, it is called unstable. The eigenvalues of a Jacobian matrix identify the stability of a system. If all the eigenvalues have negative real parts for a particular operating parameter (say the amount of heat input), then the system is known as a stable system. On the other hand, if at least one eigenvalue has a positive real part, then the system is unstable for that operating parameter. The Jacobian matrix used to identify the eigenvalues and judge stability is formed from Equations (6)-(8). The eigenvalues are calculated based on the characteristic equation,

$$|\boldsymbol{J} - \lambda\boldsymbol{I}| = 0 \tag{22}$$

where λ is the eigenvalues and $\boldsymbol{I}$ the identity matrix.

A stability boundary separates a stable region from an unstable region when sweeping across operating parameters. In the present work, the eigenvalues on the stable and unstable sides of the stability boundary are complex (i.e., $\lambda = \lambda_R \pm i\omega$, where the sign of λ_R determines the stability as discussed above). So, at the stability boundary, the eigenvalues are purely imaginary (i.e., $\lambda = 0 \pm i\omega$). A stability boundary having purely imaginary eigenvalues is one indication of a particular type of bifurcation called a Hopf bifurcation. At a bifurcation, the qualitative behavior (i.e., diverging to converging or vice-versa) or number equilibrium points of a dynamical system changes when an operating parameter changes. The significance of Hopf bifurcation is that it

indicates an oscillating limit cycle will arise for a particular dynamical system [36,37]. A dynamical system is confirmed to have a Hopf bifurcation at some specific parameter M_c if it satisfies the following two conditions at that parameter: i) has purely imaginary eigenvalues $\lambda = \pm i\omega$; and ii) $\frac{d\lambda_R}{dM_C} \neq 0$.

2.4 Transient solution of oscillation dynamics

In this work, the system stability boundaries are assessed for parameter changes in the heat input, mass flux, and amount of inlet restriction. Both conditions for a Hopf bifurcation are confirmed in the present system, which indicates the occurrence of pressure drop oscillations in the unstable regions of the stability maps. The characteristics of transient system oscillations are then predicted in these unstable regions. In order to obtain the transient solutions, the set of ordinary differential Equations (6) and (8) are numerically solved using MATLAB (ODE15s), as these equations are stiff. The solution method is a variable-step, variable-order (VSVO) solver based on the numerical differentiation formulas (NDF) of orders 1 to 5. This solves the equations as initial values problems (IVP), and the initial values are perturbed equilibrium points ($P_{buf}^* \pm \delta P_{buf}, G_{in}^* \pm \delta G_{in}$).

3   Results and Discussions

The bifurcation analysis results are first shown as parametric stability maps, followed by detailed descriptions of the oscillatory system mass flux dynamics for operating points in the unstable region. Lastly, the characteristic period and amplitude of these pressure drop oscillations, as well as the damping effects of inlet throttling, are mapped over the parameter space and discussed.
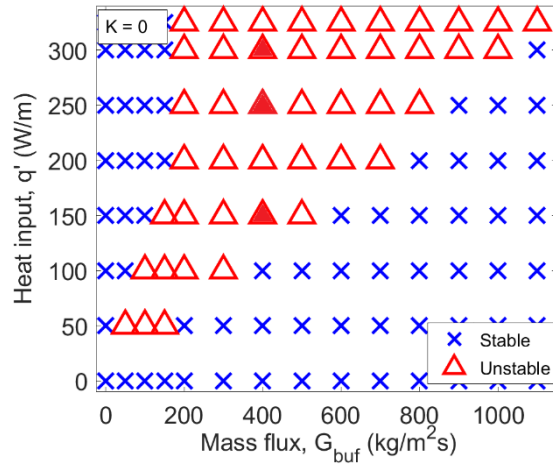
3.1   Stability map

Stability maps are first generated by calculating the eigenvalues over parameter sweeps of the heat input and mass flux from 0-325 W/m and 0-1100 kg/m^{2}s, respectively, with no inlet throttling. The other system parameters are fixed as given in Table 1.

Figure 3(a) shows the stable and unstable regions of the microchannel in this parametric plane of mass flux and heat input by labeling the discrete stability points. Notably, at a given heat input, the system exhibits two stable regions at high and low mass fluxes, with an unstable region in between. As introduced earlier, the stable region at higher mass fluxes occurs because there is only subcooled liquid inside the channel. Similarly, the stability of the channel at a significantly lower mass fluxes is because the channel is filled with superheated vapor along most of the length; the single-phase vapor flow characteristics dominate the behavior. The unstable region corresponds to the intermediate mass flux range over which the channel pressure drop demand curve is inversely proportional to the mass flux in a two-phase flow region. For a given mass flux, there is a minimum heat input below which the system has a stable nature because the applied heat input is insufficient to saturate the flow, which remains a single liquid phase. With increasing heat input, the fluid becomes saturated and generates a liquid-vapor mixture in the channel over a broader range of mass fluxes, leading to a broader unstable region.

To assess the influence of inlet throttling, Figure 3(b) shows a stability map in the parametric plane of the resistance coefficient and mass flux, for a fixed heat input $q' = 300$ W/m. The effect of mass flux on stability without throttling ($K = 0$) matches the behavior and regions as discussed above. The stability boundaries at low and high mass fluxes converge with increasing inlet throttling, narrowing the unstable region; at a certain throttling ($K > 1000$), the unstable region vanishes, and the system is stable across all mass fluxes. This map illustrates the effect of throttling to stabilize two-phase operation, a phenomenon known in the literature [14].

The two stability maps in Figure 3 are useful to identify the stable and unstable regions, but they do not offer insight into the nature of the system dynamics in the unstable regions (in this case, pressure drop oscillations). The following subsections explore in detail these transient dynamics as a function of heat input and throttling, as well as mapping of the period and amplitude of pressure drop oscillations that occur.

(a)
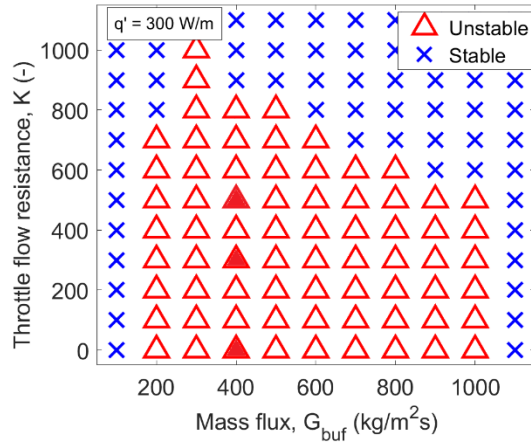
(b)

Figure 3 Stability map for the microchannel heat sink system in parametric planes of (a) heat input versus mass flux without inlet throttle ($K = 0$) and (b) inlet throttling versus mass flux for heat input q' =300 W/m. The symbols noted in the legends differentiate the stable region (converging nature) and unstable region (diverging nature), with the stability boundary between. The filled symbols indicate the specific unstable operating points at which the transient pressure drop oscillation dynamics are described in Sections 3.2 and 3.3.

3.2   Effect of heat input on oscillation dynamics

The effect of heat input on the transient oscillations is analyzed for several representative cases within the unstable region at a fixed nominal mass flux of $G_{buf} = 400$ kg/m²s and no inlet

throttling. Specifically, the transient dynamics are predicted at the operating points of the parameter space indicated by filled triangles in Figure 3(a).

At heat inputs below 150 W/m, the system is stable and any disturbance to the system results in converging oscillations of mass flux that return the system to the initial operating equilibrium point. Above this heat input, in the unstable region, a disturbance to the system leads to diverging oscillations in mass flux that eventually reach a time-periodic limit cycle. Figure 4(a) plots these time-periodic oscillations in mass flux at three increasing heat inputs (150 W/m, 250 W/m, and 300 W/m); a horizontal dashed reference line indicates stable operation at 400 kg/m^{2}s associated with lower heat inputs. It is evident from the figure that the amplitude of the oscillations increases with increasing heat input. Higher heat inputs can evaporate more liquid inside the microchannel and hence generate more vapor at the same fixed mass flux, leading to this increased amplitude compared to lower heat inputs. The frequency of oscillations also becomes smaller, or the period longer, at higher heat inputs. As a result, during these oscillations, the duration over which the channel is flow starved at a low mass flux (with a single vapor phase outlet) becomes longer. This extended time at a very low mass flux is likely to reduce the time-averaged heat transfer coefficient and increases risk that the system may experience a premature critical heat flux (i.e., a permanent temperature runaway due to formation of a stable vapor film over the heat surface). The amplitude and period of these oscillations can therefore be considered a metric for the severity of their impact on the heat transfer performance.

Figure 4(b) plots the time-periodic limit cycle of the pressure drop oscillations for two selected heat inputs of 150 W/m and 300 W/m. Specifically, a solid line traces the dynamic path of the pressure drop ($\Delta P = P_{buf} - P_{atm}$) versus channel mass flux G_{in}, with an arrow indicating the direction of the cycle; because there is no inlet throttle in this case, the buffer tank pressure is equivalent to the pressure rise above ambient across the channel. At each heat input, the limit cycle overlays a dashed line indicating the channel demand curve for the system. The demand curve at a given heat input has the typical non-monotonic N-shaped curve associated with flow boiling. The negative slope in the two-phase region at 400 kg/m^{2}s become steeper for higher heat input. During the oscillations, the microchannel periodically shifts between a single-phase liquid outlet (at high mass fluxes on the right side) and single-phase vapor outlet (at low mass fluxes on the left side).

The periodic oscillations follow the same trajectory as discussed in Figure 1(a), per the mechanism of pressure drop oscillations discussed in the introduction section.
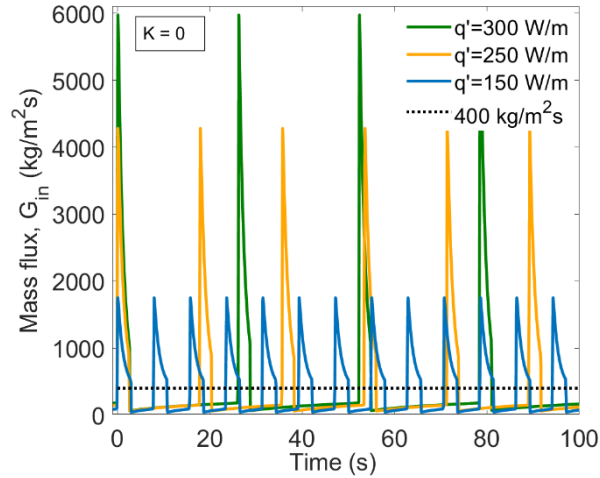

(a)
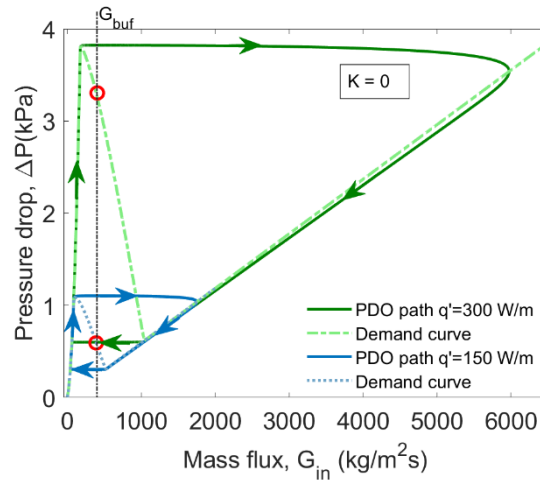
(b)

Figure 4 (a) Temporal variation of mass flux due to pressure drop oscillations in the unstable region ($G_{buf} = 400$ kg/m^{2}s for $q' = 150$ W/m, 250 W/m, and 300 W/m; $K = 0$; locations of these operating points indicated by filled triangles in Figure 3(a)). (b) Limit cycle path of pressure drop versus channel mass flux overlaid on channel demand curve.

The period and amplitude of these oscillations are calculated over the complete range of mass fluxes and heat inputs. Figure 5 shows the parametric plane of heat input and mass flux over the

same range as the previously discussed stability map (Figure 3(a)), where the color assigned to each point indicates the amplitude (Figure 5(a)) and period (Figure 5(b)) of the pressure drop oscillations. It is noted from the Figure 5(a) that the amplitude of oscillations directly corresponds with an increasing heat input. At lower heat input, say 50 W/m, while there exists an unstable region, the amplitude of oscillations is very mild and may not have significant impact on the heat transfer performance. With higher heat input, the amplitude of oscillations can increase dramatically, over thirty-five times greater at 300 W/m versus 50 W/m for example. Interestingly, at a given heat input, the mass flux has no effect on the amplitude; as soon as the system enters into the unstable region through either stability boundary, oscillations occur with the same amplitude. Conversely, the period of oscillations shown in Figure 5(b) is affected by both the heat input and mass flux. Similar to the amplitude, the period of oscillations increases with increasing heat input. However, the period of oscillations is also determined by the mass flux and becomes longer with decreasing mass flux.

Compared to a stability diagram that only labels the regions of stability, these contour plots provide critical insight into potential effects of the pressure drop oscillations on heat transfer performance. The significance of identifying the amplitude and period of oscillations is that their severity is expected to correspond to the heat transfer coefficient deterioration and vulnerability to critical heat flux. Moreover, the frequency and period of the oscillations may have possible impact via thermal cycling or vibration of system components. Hence, these results indicate that operation at either lower mass flow rate or increasing heat inputs generally makes systems more susceptible to these deleterious effects.
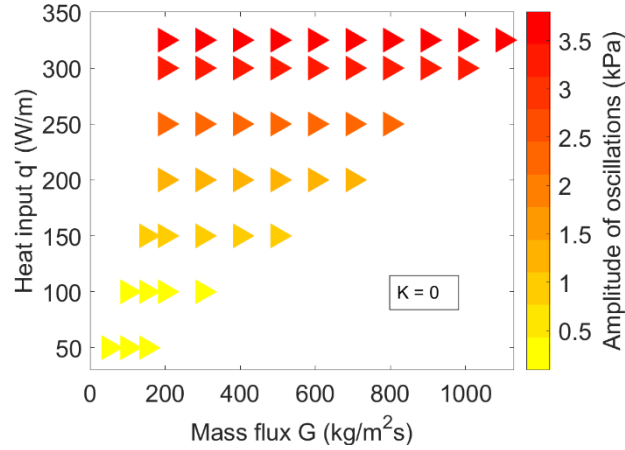
(a)
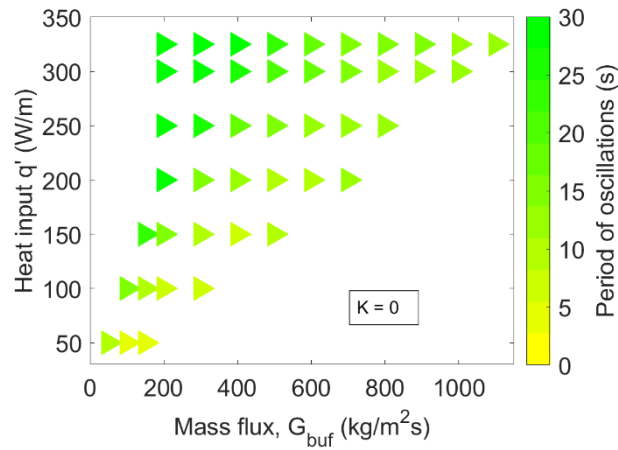
(b)

Figure 5 Pressure drop oscillation (a) amplitude and (b) period in the parametric plane of heat input versus mass flux for inlet throttle K=0. The color of each unstable point maps to the contour scales shown; stable points having zero oscillation amplitude are excluded.

## 3.3 Effect of inlet throttling on oscillation dynamics

While inlet throttling is known to generally stabilize these flow boiling systems, previous studies typically investigate a fixed inlet throttling or do not interrogate their effect on the period or amplitude of pressure drop oscillations. This section uses the same data presentation established in Section 3.2 above to describe the effect of inlet throttling on these behaviors of pressure drop oscillations in detail.

23

The effect of inlet throttling on the time-periodic oscillations of mass flux inside the channel are shown in Figure 6(a). The time evolution of mass flux is plotted for cases of three different inlet throttling resistance coefficients of $K = 100$, 300, and 500, at a nominal mass flux of $G_{buf} = 400$ kg/m^{2}s and constant heat input of $q' = 300$ W/m, all within the unstable region (operating points indicated with filled triangles in Figure 3(b)). While the important effect of inlet restriction on narrowing the unstable region was previously shown in the stability map, this result is the first to illustrate that the amplitude of oscillations decreases and the period of oscillations shortens as the throttling is increased within the unstable region. This trend can be explained by inspecting the pressure drop oscillation limit cycle plotted in Figure 6(b), overlaid on the demand curves of the combined channel and orifice system.

The system demand curve with the lowest throttling $K = 0$ has a two-phase mixture region that spans a much broader range of mass flux (177-1043 kg/m^{2}s) and pressure drop (0.62-3.82 kPa). This two-phase mixture region generally gets narrower with increasing throttling. For the higher throttling at $K = 500$, this region spans significant smaller ranges of mass flux (190-1021 kg/m^{2}s) and pressure drop (2.95-3.88 kPa). Hence, the limit cycle must only traverse this shorter range of mass fluxes, leading to the lower amplitude of oscillations. The same reasoning explains the shortened period of oscillations, as it takes less time to complete one cycle. As discussed previously, this reduction of severity in the oscillations is likely to have associated benefits in the heat transfer performance of the system, meaning that inlet restrictors provide benefit within the unstable region even if they do not completely suppress the instability. Also, if the concern is primarily regarding vibrations associated with these oscillations in some system, with degradation mechanisms known to occur at a specific frequency, inlet throttling may be used to tune away from this frequency.
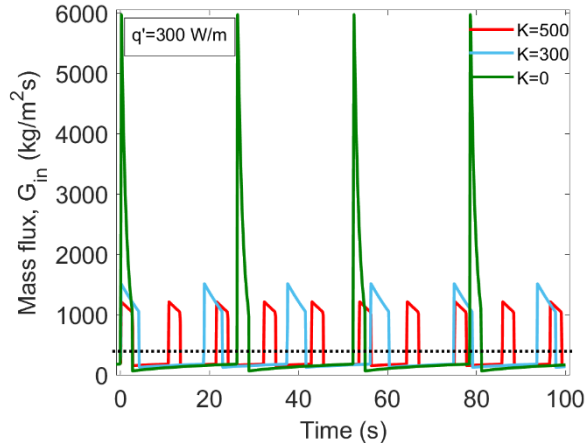
(a)
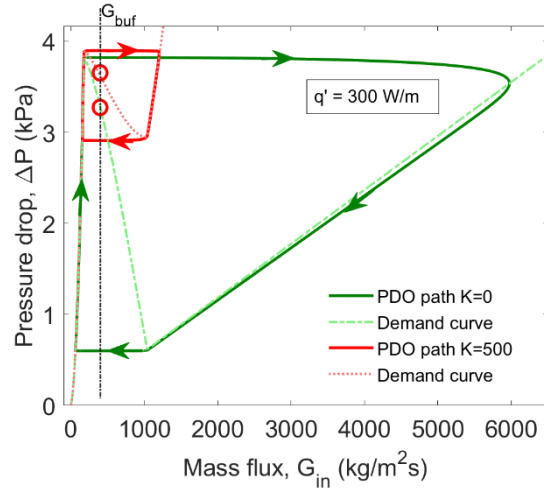
(b)

Figure 6 Temporal variation of mass flux due to pressure drop oscillations in the unstable region (G_{buf} = 400 kg/m²s for K = 0, 300, and 500; q' = 300 W/m; locations of these operating points indicated by filled triangles in Figure 3(b)). (b) Limit cycle path (solid line) of pressure drop versus channel mass flux overlaid on channel demand curve.

To assess the impact of inlet restriction over the complete range of operation at a constant heat input q'=300 W/m, Figure 7 plots the pressure drop oscillation amplitude (Figure 7(a)) and period (Figure 7(b)) throughout the parametric plane of throttling resistance coefficients and mass fluxes from the stability map shown earlier in Figure 3(b). The color of each point denotes the amplitude and period of oscillations. It is evident from Figure 7(a) that the amplitude of oscillations is decreases with increasing inlet throttling across the complete range of mass fluxes; the stabilizing

effect of higher inlet throttling on the magnitude of the amplitude is also consistent across all mass fluxes. Conversely, Figure 7(b) shows that the shortening of the period with increasing mass flux is most effective over an intermediate range of mass fluxes. Near the stability boundary at very low and high mass fluxes, while there is a resistance coefficient above which the system is fully stable, once the system enters into the unstable region with a decreasing resistance coefficient, the there is little effect of throttling on the period.
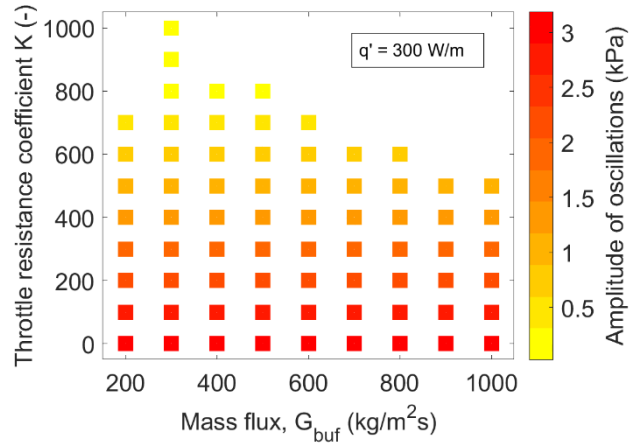
(a)
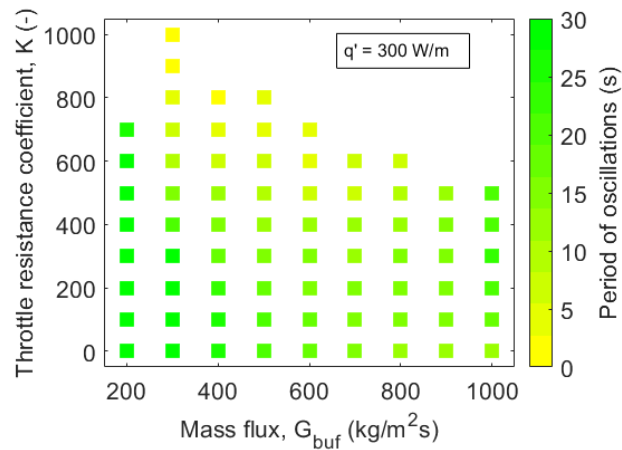
(b)

Figure 7. Pressure drop oscillation (a) amplitude and (b) period in the parametric plane of inlet throttle versus mass flux for heat input $q' = 300$ W/m. The color of each unstable point maps to the contour scales shown; stable points having zero oscillation amplitude are excluded.

.

Overall, an increasing amount of inlet throttling is beneficial in terms of both the amplitude and period of oscillations, rendering the microchannel less prone to reduction in heat transfer performance as the stability boundary is approached. This work motivates future study of the specific relationship between the oscillation severity and such deleterious effects in the heat transfer coefficient or critical heat flux. For example, the work of Park et al. [38] has experimentally shown the affect of flow oscillation (not necessarily due to pressure drop oscillations) on heat transfer coefficient during flow boiling. They identified a threshold amplitude and period above which oscillations can deteriorate the heat transfer coefficient, and that the amount of deterioration depends on amplitude and period of oscillations. Given specific targets for the amplitude or period below which performance is unaffected, this modeling framework could be used to more precisely design inlet restrictors that impose less pressure drop penalty than required for full suppression of the instability.

4   Conclusion

The dynamic flow instability mechanism of pressure drop oscillations is investigated for microchannel flow boiling heat sink systems. Pressure drop oscillations occur when the pressure drop versus mass flux demand curve of the channels has the characteristic non-monotonic shape associated with flow boiling, along with an upstream compressible volume. A dynamic model is developed for analyzing the pressure drop oscillations and assessing the system stability. Stability maps are generated over ranges of different operating parameters (heat inputs q' from 0-325 W/m, mass fluxes G_{buf} from 0-1100 kg/m²s, and inlet restriction resistance coefficients K from 0-1100) using bifurcation analysis. Investigation of these maps recovers several typical stability characteristics of such systems. Namely, at higher heat inputs (q'=325 W/m), the system generally has a narrower region of mass fluxesover which operation is stable (e.g.,, a stable region from G_{buf}=0-200 kg/m²s and unstable region from G_{buf}=200-1100 kg/m²s). Inlet restrictors act to stabilize the system and broaden this stable region with higher flow resistance coefficients (e.g., at K=1100, the unstable region vanishes, and the system becomes stable).

While the stability map is useful for determining the occurrence of instabilities, it offers no insight into the behavior of the pressure drop oscillations in the unstable region. Of particular

interest is predicting and understanding the severity of the amplitude and period of pressure drop oscillations, which serve as proxy metrics for the potential deleterious effects on the heat transfer performance. Oscillations in mass flux are known to affect the heat transfer coefficient and longer periods of flow starvation are more likely to induce premature critical flux. The dynamic model is therefore solved to predict the unstable limit cycle and analyze these dynamic pressure drop oscillation characteristics. The amplitude and period of pressure drop oscillations are plotted over the unstable region, quantitatively mapping how their severity generally increases with increasing heat input, reducing mass flux, and reducing inlet restriction. This reveals a new design space in which pressure drop oscillations may be tolerable, even within the unstable region, due to having a sufficiently low amplitude or high frequency; inlet restrictors can be used tune these oscillation dynamics to meet specific design criteria. This modeling framework motivates future work that could predictively map the effects of the oscillation dynamics on heat transfer performance over the same parametric space.

References

[1]   S. Kakac, B. Bon, A Review of two-phase flow dynamic instabilities in tube boiling systems, Int. J. Heat Mass Transf. 51 (2008) 399–433. https://doi.org/10.1016/j.ijheatmasstransfer.2007.09.026.

[2]   L.E. O'Neill, I. Mudawar, Review of two-phase flow instabilities in macro- and micro-channel systems, Int. J. Heat Mass Transf. 157 (2020) 119738. https://doi.org/10.1016/j.ijheatmasstransfer.2020.119738.

[3]   S. Lee, V.S. Devahdhanush, I. Mudawar, Experimental and analytical investigation of flow loop induced instabilities in micro-channel heat sinks, Int. J. Heat Mass Transf. 140 (2019) 303–330. https://doi.org/10.1016/j.ijheatmasstransfer.2019.05.077.

[4]   W. Qu, I. Mudawar, Measurement and prediction of pressure drop in two-phase micro-channel heat sinks, Int. J. Heat Mass Transf. 46 (2003) 2737–2753. https://doi.org/10.1016/S0017-9310(03)00044-9.

[5]   S.G. Kandlikar, W.K. Kuan, D.A. Willistein, J. Borrelli, Stabilization of flow boiling in microchannels using pressure drop elements and fabricated nucleation sites, J. Heat Transfer. 128 (2006) 389–396. https://doi.org/10.1115/1.2165208.

[6]   J. Pyrhönen, P. Lindh, M. Polikarpova, E. Kurvinen, V. Naumanen, Heat-transfer improvements in an axial-flux permanent-magnet synchronous machine, Appl. Therm. Eng. 76 (2015) 245–251. https://doi.org/10.1016/j.applthermaleng.2014.11.003.

[7]   Y. Ding, H. Ji, M. Wei, R. Liu, Effect of liquid cooling system structure on lithium-ion battery pack temperature fields, Int. J. Heat Mass Transf. 183 (2022) 122178. https://doi.org/10.1016/j.ijheatmasstransfer.2021.122178.

[8]   M. Ledinegg, Instability of flow during natural and forced circulation, Die Warme. 61

(1938) 891–898.

[9]   T. Van Oevelen, J.A. Weibel, S. V. Garimella, Predicting two-phase flow distribution and stability in systems with many parallel heated channels, Int. J. Heat Mass Transf. 107 (2017) 557–571. https://doi.org/10.1016/j.ijheatmasstransfer.2016.11.050.

[10]   T. Van Oevelen, J.A. Weibel, S. V. Garimella, The effect of lateral thermal coupling between parallel microchannels on two-phase flow distribution, Int. J. Heat Mass Transf. 124 (2018) 769–781. https://doi.org/10.1016/j.ijheatmasstransfer.2018.03.073.

[11]   A. Miglani, J.A. Weibel, S. V. Garimella, Measurement of flow maldistribution induced by the Ledinegg instability during boiling in thermally isolated parallel microchannels, Int. J. Multiph. Flow. 139 (2021) 103644. https://doi.org/10.1016/j.ijmultiphaseflow.2021.103644.

[12]   A. Miglani, J.A. Weibel, S. V. Garimella, An experimental investigation of the effect of thermal coupling between parallel microchannels undergoing boiling on the Ledinegg instability-induced flow maldistribution, Int. J. Multiph. Flow. 139 (2021) 103536. https://doi.org/10.1016/j.ijmultiphaseflow.2020.103536.

[13]   F. Xu, H. Wu, Effect of pin-fins on the onset of flow instability of water in silicon-based microgap, Int. J. Therm. Sci. 130 (2018) 496–506. https://doi.org/10.1016/j.ijthermalsci.2018.05.020.

[14]   N. Mao, J. Zhuang, T. He, M. Song, A critical review on measures to suppress flow boiling instabilities in microchannels, Heat Mass Transf. 57 (2021) 889–910. https://doi.org/10.1007/s00231-020-03009-2.

[15]   E. Manavela Chiapero, M. Fernandino, C.A. Dorao, Review on pressure drop oscillations in boiling systems, Nucl. Eng. Des. 250 (2012) 436–447. https://doi.org/10.1016/j.nucengdes.2012.04.012.

[16]   T. Zhang, Y. Peles, J.T. Wen, T. Tong, J.Y. Chang, R. Prasher, M.K. Jensen, Analysis and active control of pressure-drop flow instabilities in boiling microchannel systems, Int. J. Heat Mass Transf. 53 (2010) 2347–2360. https://doi.org/10.1016/j.ijheatmasstransfer.2010.02.005.

[17]   G.P. Celata, S.K. Saha, G. Zummo, D. Dossevi, Heat transfer characteristics of flow boiling in a single horizontal microchannel, Int. J. Therm. Sci. 49 (2010) 1086–1094. https://doi.org/10.1016/j.ijthermalsci.2010.01.019.

[18]   Y. Wang, K. Sefiane, Effects of heat flux, vapour quality, channel hydraulic diameter on flow boiling heat transfer in variable aspect ratio micro-channels using transparent heating, Int. J. Heat Mass Transf. 55 (2012) 2235–2243. https://doi.org/10.1016/j.ijheatmasstransfer.2012.01.044.

[19]   M.D. Clark, J.A. Weibel, S. V Garimella, Impact of pressure drop oscillations on surface temperature and critical heat flux during flow boiling in a microchannel, IEEE Trans. Components, Packag. Manuf. Technol. 11 (2021) 1634–1644. https://doi.org/10.1109/TCPMT.2021.3094767.

[20]   Y. Wang, K. Sefiane, Z. Wang, S. Harmand, Analysis of two-phase pressure drop fluctuations during micro-channel flow boiling, Int. J. Heat Mass Transf. 70 (2014) 353–

362. https://doi.org/10.1016/j.ijheatmasstransfer.2013.11.012.

[21]   M.M. Padki, K. Palmer, S. Kakaç, T.N. Veziroğlu, Bifurcation analysis of pressure-drop oscillations and the Ledinegg instability, Int. J. Heat Mass Transf. 35 (1992) 525–532. https://doi.org/10.1016/0017-9310(92)90287-3.

[22]   M.E. Rahman, S. Singh, Non-linear stability analysis of pressure drop oscillations in a heated channel, Chem. Eng. Sci. 192 (2018) 176–186. https://doi.org/10.1016/j.ces.2018.07.013.

[23]   T. Zhang, J.T. Wen, Y. Peles, J. Catano, R. Zhou, M.K. Jensen, Two-phase refrigerant flow instability analysis and active control in transient electronics cooling systems, Int. J. Multiph. Flow. 37 (2011) 84–97. https://doi.org/10.1016/j.ijmultiphaseflow.2010.07.003.

[24]   Y. Kuang, W. Wang, J. Miao, X. Yu, H. Zhang, Pressure drop instability analysis in mini-channel evaporators under different magnitudes of gravity, Int. J. Therm. Sci. 147 (2020) 105952. https://doi.org/10.1016/j.ijthermalsci.2019.05.008.

[25]   M.E. Rahman, S. Singh, Flow excursions and pressure drop oscillations in boiling two-phase channel, Int. J. Heat Mass Transf. 138 (2019) 647–658. https://doi.org/10.1016/j.ijheatmasstransfer.2019.04.025.

[26]   M.E. Rahman, S. Singh, Pressure drop oscillations with symmetry breakdown in two-phase flow parallel channels, J. Heat Transfer. 143 (2021). https://doi.org/10.1115/1.4049032.

[27]   J. Eborn, On model libraries for thermo-hydraulic applications, Lund Institute of Technology, 2001. http://www.control.lth.se/documents/2001/ebo01phd.pdf.

[28]   S. Paul, S. Paul, M. Fernandino, C.A. Dorao, The overlooked role of pressure oscillations on heat transfer deterioration during self-sustained flow oscillations, Appl. Phys. Lett. 117 (2020) 253701. https://doi.org/10.1063/5.0020361.

[29]   M.H. Rausch, L. Kretschmer, S. Will, A. Leipertz, A.P. Fröba, Density, surface tension, and kinematic viscosity of hydrofluoroethers HFE-7000, HFE-7100, HFE-7200, HFE-7300, and HFE-7500, J. Chem. Eng. Data. 60 (2015) 3759–3765. https://doi.org/10.1021/acs.jced.5b00691.

[30]   A.L. Hazel, M. Heil, The steady propagation of a semi-infinite bubble into a tube of elliptical or rectangular cross-section, J. Fluid Mech. 470 (2002) 91–114. https://doi.org/10.1017/S0022112002001830.

[31]   P. Cheng, H.Y. Wu, Mesoscale and microscale phase-change heat transfer, in: G.A. Greene, J.P. Hartnett†, A. Bar-Cohen, Y.I.B.T.-A. in H.T. Cho (Eds.), Elsevier, 2006: pp. 461–563. https://doi.org/10.1016/S0065-2717(06)39005-3.

[32]   S.M. Zivi, Estimation of steady-state steam void-fraction by means of the principle of minimum entropy production, J. Heat Transfer. 86 (1964) 247–251. https://doi.org/10.1115/1.3687113.

[33]   D. Chisholm, A theoretical basis for the Lockhart-Martinelli correlation for two-phase flow, Int. J. Heat Mass Transf. 10 (1967) 1767–1778. https://doi.org/10.1016/0017-9310(67)90047-6.

[34]   Y.S. Muzychka, M.M. Awad, Asymptotic generalizations of the Lockhart–Martinelli

method for two phase flows, J. Fluids Eng. 132 (2010) 0313021–03130212. https://doi.org/10.1115/1.4001157.

[35]   K. Mishima, T. Hibiki, Some characteristics of air-water two-phase flow in small diameter vertical tubes, Int. J. Multiph. Flow. 22 (1996) 703–712. https://doi.org/10.1016/0301-9322(96)00010-9.

[36]   S. Wiggins, Introduction to applied nonlinear dynamical systems and chaos, Springer-Verlag, New York, 2003. https://doi.org/10.1007/b97481.

[37]   S.H. Strogatz, Nonlinear dynamics and chaos: with applications to physics, biology, chemistry, and engineering, Perseus Books Publishing, Reading, Massachusetts, 1994.

[38]   I.W. Park, J. Ryu, M. Fernandino, C.A. Dorao, Can flow oscillations during flow boiling deteriorate the heat transfer coefficient?, Appl. Phys. Lett. 113 (2018) 154102. https://doi.org/10.1063/1.5046429.